Infrared Spectra of HC≡C-MH and M−η^2-(C_2H_2) from Reactions of Laser-Ablated Group-4 Transition-Metal Atoms with Acetylene

Han-Gook Cho, Gary P. Kushto,† Lester Andrews,* and Charles W. Bauschlicher, Jr.

Department of Chemistry, University of Incheon, 177 Dohwa-dong, Nam-ku, Incheon, 402-749, South Korea, Department of Chemistry, University of Virginia, P.O. Box 400319, Charlottesville, Virginia 22904-4319, and Space Technology Division, NASA Ames Research Center, Mail Stop 230-3, Moffett Field, California 94035

Received: February 14, 2008; Revised Manuscript Received: April 28, 2008

Reactions of laser-ablated group 4 transition-metal atoms with acetylene have been carried out. The ethynyl metal hydrides (HC≡C-MH) and corresponding π complexes (M−η^2-(C_2H_2)) are identified in the matrix infrared spectra. The observed M−H and C−M stretching absorptions show that oxidative C−H insertion readily occurs during codeposition and photolysis afterward. The absorptions from the π complex, on the other hand, are relatively weak in the original deposition spectrum but increase dramatically in the process of annealing. The vinylidene complex, another plausible product, is not identified in this study. The observed spectra and DFT calculations both show that the back-donations from the group 4 metals to the antibonding π^* orbital of C_2H_2 are extensive such that the group 4 metals form unusually strong π complexes. Thus, it is the formation of two Ti−C bonds in the group 4 systems than leads to the stronger bonding than that in the group 8 systems. While bonds form, the Ti atom is weakly bound to C_2H_2, and we still refer to it as a π complex. Evidence of relativistic effects is also observed in frequency trends for the Ti, Zr, and Hf products.

Introduction

Transition-metal complexes with unsaturated ligands make up an important portion of organometallic chemistry, and many of them are also industrially important, with various chemical properties including catalytic activities.[1] While numerous complexes with an acetylene ligand have been introduced, most of them include other bulky ligands to stabilize the structure. On the other hand, small π systems (e.g., M(C_2H_2)), which are the model systems for the much larger complexes containing unsaturated ligands, are relatively less studied.[2–6] While surface studies and cluster chemistry provides insights into bond cleavage and rearrangement in organometallic syntheses and transition-metal catalysis, the matrix isolation technique presents a more direct method for study of transition-metal−acetylene interactions

The small metal−acetylene complexes are mostly provided in reactions of metal atoms with acetylene[2–6] or in the hydrogen elimination reaction of ethylene by metal atoms.[7] Various structures of metal−acetylene complexes have been reported. The most plausible metal−acetylene complex is the π complex (I in Scheme 1), M−η^2-(C_2H_2),[2] with the Dewar−Chatt−Duncanson scheme of bonding.[8] The small metal π complexes known to date are mostly weak π complexes. The vinyl forms (II) and hydrogen-bonded metal−acetylene complexes (III) have also been reported.[2] The formation of Fe, Ni, and Pt C−H insertion complexes (IV), HC≡C−MH, upon UV photolysis have been discussed more recently.[3,4] Kline et al. showed that the Ni π complex shows an extreme case of π complexation, where the triple bond of acetylene reduces to a double bond, due to its strong carbon−metal bonds.[3b] Similar strong complexation is also observed for LiC_2H_2.[5] Ni and Pt also give vinylidene

SCHEME 1

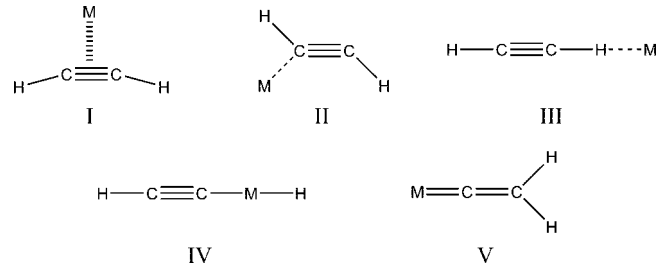

products (M═C═CH_2) (V).[3,4] In contrast laser-ablated Be, B, Al, Th, and U produce ethynyl metal hydrides, and the actinides also form strong metallacycles.[9]

In this study, group 4 metal atom (Ti, Zr, and Hf) reactions with acetylene have been carried out in excess argon, and the products are identified in the matrix IR spectra. All three metals readily form ethynyl metal hydride complexes (HC≡C−MH) via oxidative C−H insertion during codeposition and photolysis afterward. The product spectra also show formation of the π complexes, and their low C−C stretching frequencies suggest that the back-donation is much more extensive in comparison with those of the previously studied transition-metal π complexes.[2,4–7] The products are identified by using isotopomers and DFT calculations.

Experimental and Computational Methods

Laser-ablated Ti (Goodfellow), Zr, and Hf (Johnson−Matthey) atoms were reacted with C_2H_2 (Matheson, passed through a series of traps to remove acetone stabilizer), C_2D_2, and $^{13}C_2H_2$ (Cambridge Isotopic Laboratories, 99%) in excess argon during condensation at 8 K using a closed-cycle refrigerator (Air Products HC-2). These methods have been described in detail elsewhere.[10] Reagent gas mixtures ranged from 0.1 to 0.5% in argon. After reaction, infrared spectra were recorded at a

* To whom correspondence should be addressed. E-mail: lsa@virginia.edu.

† Present address: Optical Sciences Branch, United States Naval Research Laboratory, Washington, DC 10375.

10.1021/jp801336d CCC: $40.75
Published on Web 07/10/2008

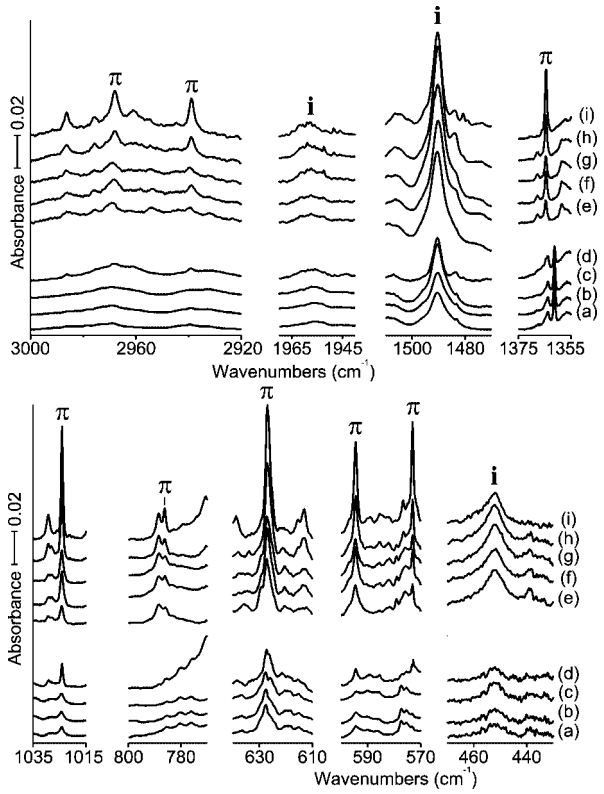

Figure 1. IR spectra in the product absorption regions for laser-ablated Ti atoms codeposited with C_2H_2 in excess argon at 8 K and their variation. (a) Ti + 0.5% C_2H_2 in Ar codeposited for 1 h. (b) As that in (a) after photolysis ($\lambda > 420$ nm). (c) As that in (b) after photolysis ($240 < \lambda < 380$ nm). (d) As that in (c) after annealing to 36 K. (e) Ti + 0.5% C_2H_2 in Ar codeposited for 1 h. A laser power three times as high is used. (f) As that in (e) after annealing to 24 K. (g) As that in (f) after 30 min photolysis ($\lambda < 220$ nm). (h) As that in (g) after annealing to 29 K. (i) As that in (h) after annealing to 35 K. Here, **i** and $\boldsymbol{\pi}$ denote the product absorption group.

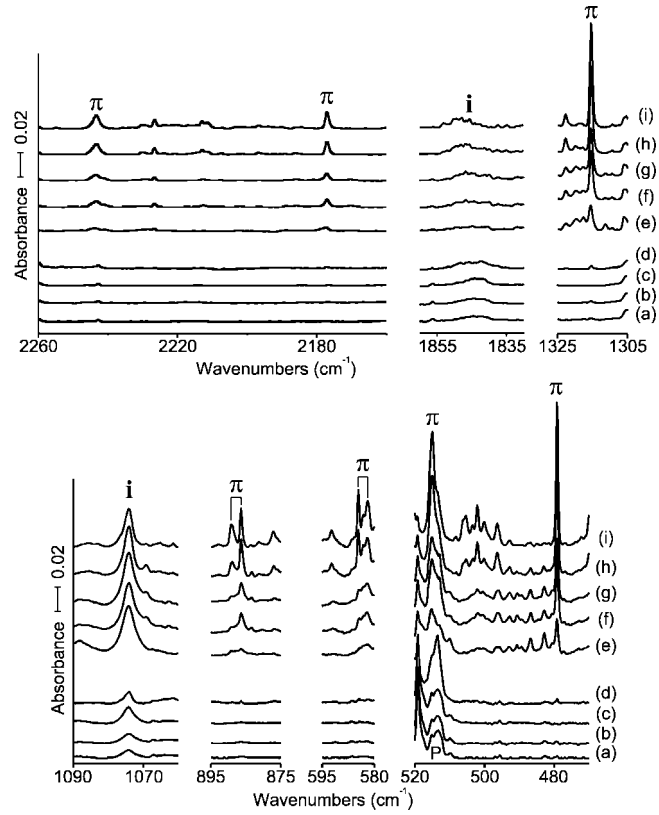

Figure 2. IR spectra in the product absorption regions for laser-ablated Ti atoms codeposited with C_2D_2 in excess argon at 8 K and their variation. (a) Ti + 0.5% C_2D_2 in Ar codeposited for 1 h. (b) As that in (a) after photolysis ($\lambda > 420$ nm). (c) As that in (b) after photolysis ($240 < \lambda < 380$ nm). (d) As that in (c) after annealing to 36 K. (e) Ti + 0.25% C_2D_2 in Ar codeposited for 2 h. A laser power three times as high is used. (f) As that in (e) after annealing to 24 K. (g) As that in (f) after 30 min photolysis ($\lambda < 220$ nm). (h) As that in (g) after annealing to 29 K. (i) As that in (h) after annealing to 35 K. Here, **i** and $\boldsymbol{\pi}$ denote the product absorption group.

resolution of 0.5 cm^{-1} using a Nicolet 550 spectrometer with an MCT-B detector. Samples were later irradiated for 20 min periods (except where otherwise noted) by a mercury arc street lamp (175 W) with the globe removed and a combination of optical filters and subsequently annealed to allow further reagent diffusion.

Complementary density functional theory (DFT) calculations were carried out using the Gaussian 03 package,[11] B3LYP density functional,[12] 6-311++G(3df,3pd) basis sets for C, H, and Ti, and SDD pseudopotential and basis set[13] for Zr and Hf to provide a consistent set of vibrational frequencies for the reaction products. Geometries were fully relaxed during optimization, and the optimized geometry was confirmed by vibrational analysis, and BPW91[14] calculations were also done to confirm the B3LYP results. The vibrational frequencies were calculated analytically, and the zero-point energy was included in the calculation of binding energy of a metal complex.

Results and Discussion

Reactions of Ti, Zr, and Hf with acetylene isotopomers were carried out, and the matrix infrared spectra and their variation upon photolysis and annealing will be compared with the vibrational characteristics calculated by density functional theory. In addition, bands from precursor irradiation common to other metal experiments were also observed.[4]

Ti + C_2H_2. Figures 1 and 2 show the Ti + C_2H_2 and Ti + C_2D_2 spectra and their variation in the product absorption regions. Two sets of product absorptions marked "**i**" and "$\boldsymbol{\pi}$" are observed on the basis of the variations upon photolysis and annealing. The **i** absorptions increase about 20 and 60% upon visible ($\lambda > 420$ nm) and UV ($240 < \lambda < 380$ nm) irradiations (Figures 1a–c and 2a−c), respectively. They sharpen up in the

TABLE 1: Frequencies of Product Absorptions Observed from Reactions of Ti with Acetylene Isotopomers in Excess Argon[a]

	C_2H_2	C_2D_2	$^{13}C_2H_2$	CHCD	description
$\boldsymbol{\pi}$	2968.0	2243.3	2957.1	2960.5	A_1 C−H str.
	2938.9	2177.1	2930.8	2199.5	B_2 C−H str.
	1364.6	1315.4	1312.5	1339	A_1 C−C str.
	1024.1	886.4	1007.0	970.0	B_2 HCCH bend
	786.2		785.5		A_1 HCCH bend
	627.0	582.1	623.6	653.7	B_1 HCCH bend
	594.5	515.0	580.3		A_1 TiC_2 str.
	573.0	479.2	559.2		B_2 TiC_2 str.
i	1956.1	1845.7	1888.6		A′ C−C str.
	1490.4	1074.1	1490.4	1490.4, 1074.1	A′ Ti−H str.
	672.1		666.8		A′ CCH bend
	452.6	423.5	444.8		A′ C−Ti str.
$\boldsymbol{\pi}$ + **A**	1434.4	1373.6	1384.5		C−C str.
	1050.9	901.0	1033.8		HCCH bend
i + **A**	1441.4	1037.5	1441.4		Ti−H str.

[a] All frequencies are in cm^{-1}. Description gives the major coordinate; $\boldsymbol{\pi}$ and **i** stand for the π complex and insertion products, respectively, and **A** represents acetylene.

TABLE 2: Calculated Fundamental Frequencies of HC≡C−TiH Isotopomers in the Ground $^3A''$ Electronic State[a]

	HC≡C−TiH				DC≡C−TiD				$H^{13}C{\equiv}{}^{13}C$−TiH			
approximate description	obs	BPW91	B3LYP	int.	obs	BPW91	B3LYP	int.	obs	BPW91	B3LYP	int
A′ C−H str.		3371.9	3437.7	34		2592.7	2647.2	15		3354.9	3420.3	34
A′ C−C str.		1960.9	2019.5	9		1843.4	1895.1	18		1890.1	1946.7	8
A′ Ti−H str.	1490.4	1581.7	1540.7	443	1074.1	1130.7	1101.3	235	1490.4	1581.7	1540.7	443
A′ CCH bend	672.3	661.0	701.2	43		524.6	555.6	18	666.8	654.8	694.4	44
A′ C−Ti str.	452.6	485.7	444.3	195	423.5	459.1	428.1	109	444.8	477.4	435.5	201
A′ CTiH bend		390.0	351.0	118		305.9	275.9	92		385.4	347.4	109
A′ CCTi bend		142.0	146.7	23		127.3	129.1	20		137.8	142.5	21
A″ CCH bend		667.8	671.0	50		528.4	531.0	21		661.4	664.7	51
A″ CCTi bend		146.8	174.3	28		136.0	163.3	33		142.2	168.6	26

[a] Frequencies and intensities are computed with 6-311++G(3df, 3pd) for harmonic calculations, and the all-electron basis set is used for Ti. Frequencies and intensities are in cm^{-1} and km/mol, and intensities are calculated with B3LYP. The symmetry notations are based on the C_s structure.

early stage of annealing (Figures 1 and 2d) and later decrease. The π absorptions remain unchanged upon visible irradiation but decrease about 40% on UV photolysis. They, however, increase substantially in the process of annealing. Four other absorptions at 1446.3, 1441.4, 1434.4, and 1050.9 cm^{-1} increase even more upon annealing, and they are not changed upon irradiation. One study was done with a mixed H, D sample prepared from enriched water and calcium carbide,[5] and new absorptions were observed. The most significant of these is a 1339 cm^{-1} shoulder that increases with the π absorptions upon annealing. The strong **i** absorptions were not shifted. Comparable carbon-13 experiments were performed, and the spectra are similar to those for the normal isotopic samples. The observed frequencies of the product absorptions are listed in Table 1.

The strongest **i** absorption is observed at 1490.4 cm^{-1}, and the D and ^{13}C counterparts are observed at 1074.1 and 1490.4 cm^{-1} (H/D and 12/13 ratios of 1.388 and 1.000), which are just above the TiH_2 and TiD_2 frequencies of 1435.5 and 1041.1 cm^{-1}.[15] The latter molecules also increase upon annealing here. Observation of new Ti−H and Ti−D stretching absorptions indicates that oxidative C−H insertion of acetylene occurs readily during codeposition of the metal with acetylene and photolysis afterward. The new single strong absorption is assigned to the Ti−H stretching mode of HC≡C-TiH.

Another strong **i** absorption is observed at 452.6 cm^{-1}, and the D and ^{13}C counterparts at 423.5 and 444.8 cm^{-1} (H/D and 12/13 ratios of 1.069 and 1.018). They are designated to the C−Ti stretching mode on the basis of the frequency and relatively small isotopic shifts. The **i** absorption at 1956.1 cm^{-1} shows D and ^{13}C shifts of 110.4 and 67.5 cm^{-1} (H/D and 12/13 ratios of 1.060 and 1.036), and it is assigned to the C−C stretching mode on the basis of the high frequency and sizable ^{13}C shift. A weak **i** absorption at 672.3 cm^{-1} (not shown) with the ^{13}C counterpart at 666.8 cm^{-1} (12/13 ratio 1.008) is assigned to the A′ CCH bending modes. The observed frequencies are compared with DFT frequencies for HC≡C−TiH in Table 2.

The π absorptions are, in general, much weaker than the Ti−H and C−Ti stretching absorptions of HC≡C−TiH, as shown in Figures 1a–d and 2a−d. In an effort to investigate the product responsible for the π absorptions, a laser power three times as high is used in a separate trial, which was done in the order of deposition, annealing at 24 K, full arc ($\lambda > 220$ nm) photolysis, and annealing at higher temperatures (Figures 1e–i and 2e−i). The π absorptions double upon the initial annealing at 24 K but decrease almost 50% upon photolysis. They recover and increase further in annealing at higher temperatures.

One experiment was performed for us by Manceron using thermal Ti atoms and methods described previously.[16] The π absorptions were observed upon sample deposition without the strong **i** peak. However, Xe/Hg arc irradiation depleted the π absorptions and produced the strong **i** peak. Subsequent annealing replaced the π absorptions.

The observed frequencies of the π absorptions are compared with the DFT frequencies calculated for the Ti−acetylene π complex (Ti−η^2-(C_2H_2)) in Table 3, showing that the IR-active bands of the π complex are all observed and the frequencies are consistent with the predicted values. Using a C_2H_2, CHCD, C_2D_2 reagent, the three C−C stretching modes were observed at 1364.6, 1339, and 1315.4 cm^{-1}, with the relationship predicted for this symmetrical complex. Furthermore, the C−H and C−D stretching modes for Ti−η^2-(C_2HD) are near the medians for the two pure isotopic modes, as predicted. It is notable that the C−C stretching frequency of the Ti−acetylene π complex (Ti−η^2-(C_2H_2)) is unusually low (1364.6 cm^{-1}) in comparison with those (1655, 1600.9, 1647.4, and 1658.4 cm^{-1}) of the previously studied strong Li−, Fe−, Ni−, and Pt−acetylene π complexes.[3–5] The observed C−Ti stretching frequencies of 594.5 and 573.0 cm^{-1} are, on the other hand, higher than previously reported values of 548.6, 545.3, and 539.6 cm^{-1} for Ni−η^2-(C_2H_2). This reveals that the back-donation of the Ti dπ electron to the anti-bonding π^* orbital of acetylene is unusually extensive in the Ti π complex, strengthening the C−Ti bond while weakening the C−C triple bond of acetylene. The oxidative addition of subvalent transition-metal reagents to a double or triple bond (C═C, C≡C, C═O, or C═N), with formation of three-membered metallacyles, has been termed epimetalation.[17]

The calculated absorption intensities for Ti−η^2-(C_2H_2) are weaker relative to the strong Ti−H and C−Ti stretching bands of the insertion complex (HC≡C−TiH). On the basis of the calculated and observed intensity ratios, the production yields of the insertion and π complexes during codeposition are estimated to be comparable, although the π absorptions appear weaker than the strong **i** absorptions in Figures 1 and 2. The decreasing π absorptions upon UV photolysis and the increasing **i** absorptions suggest that the π complex coverts to the insertion complex. This result is also consistent with the previous studies of Ni and Pt reactions with acetylene,[3,4] where rearrangements of the π complex to the insertion and vinylidene products are observed upon photolysis.

$$\text{Ti}-\eta^2\text{-}(\text{C}_2\text{H}_2) \xrightarrow{\text{UV}} \text{HC}\equiv\text{C}-\text{TiH}$$

The 1446.3 and 1434.4 cm^{-1} bands show slightly less carbon participation (12/13 ratio 1.03604) and more hydrogen (H/D ratio 1.04426) than the strong 1364.6 cm^{-1} band, but they are

TABLE 3: Calculated Fundamental Frequencies of Ti−C_2H_2 Isotopomers in the Ground $^3A_2$ Electronic State[a]

	Ti(C_2H_2)				Ti(C_2D_2)				Ti($^{13}C_2H_2$)				Ti(CHCD)			
approximate description	obs	BPW91	B3LYP	int.	obs	BPW91	B3LYP	int.	obs	BPW91	B3LYP	int.	obs	BPW91	B3LYP	int.
A_1 C−H str.	2968.0	3082.5	3145.0	39	2243.3	2305.7	2354.3	3	2957.1	3070.7	3132.8	42	2960.5	3068.6	3130.8	28
A_1 C−C str.	1364.6	1409.1	1467.0	86	1315.4	1354.8	1409.8	89	1312.5	1357.8	1413.5	78	1339	1382.0	1438.4	87
A_1 HCCH bend	786.2	765.1	798.7	47	582.1	589.8	559.4	37	785.5	764.3	797.7	48	653.7	664.9	686.1	26
A_1 TiC_2 str.	594.5	591.5	601.9	18		541.1	605.8	1	580.3	576.9	587.3	16		589.4	599.1	19
A_2 HCCH bend		874.8	926.7	0		697.2	738.9	0		865.6	917.0	0		811.7	859.0	9
B_1 HCCH bend	627.0	627.1	655.5	69	479.2	476.6	497.7	46	623.6	623.5	651.8	67		526.3	550.5	48
B_2 C−H str.	2938.9	3053.9	3115.9	15	2177.1	2245.0	2290.1	6	2930.8	3044.8	3106.7	16	2199.5	2275.5	2322.5	4
B_2 HCCH bend	1024.1	1023.6	1065.1	33	886.4	885.0	915.3	11	1007.0	1005.2	1046.4	34	970.0	971.5	1009.9	30
B_2 TiC_2 str.	573.0	581.8	572.5	37	515.0	498.2	492.9	36	559.2	568.5	559.2	35		512.0	510.5	36

[a] Frequencies and intensities are computed with 6-311++G(3df, 3pd) for harmonic calculations, and the all-electron basis set is used for Ti. Frequencies and intensities are in cm^{-1} and km/mol, and intensities are calculated with B3LYP. The symmetry notations are based on the C_{2v} structure.

Figure 3. IR spectra in the product absorption regions for laser-ablated Zr atoms codeposited with C_2H_2 in excess argon at 8 K and their variation. (a) Zr + 0.5% C_2H_2 in Ar codeposited for 1 h. (b) As that in (a) after photolysis ($\lambda > 420$ nm). (c) As that in (b) after photolysis ($240 < \lambda < 380$ nm). (d) As that in (c) after annealing to 36 K. (e) Zr + 0.25% C_2H_2 in Ar codeposited for 1.5 h. A laser power three times as high is used. (f) As that in (e) after annealing to 24 K. (g) As that in (f) after 30 min photolysis ($\lambda < 220$ nm). (h) As that in (g) after annealing to 28 K. (i) As that in (h) after annealing to 34 K. Here, **i** and $\boldsymbol{\pi}$ denote the product absorption group.

still mostly C−C stretching modes, and the associated 1050.9 cm^{-1} band is due to a HCCH bending mode like the 1024.1 cm^{-1} absorption. The 1434.4 and 1050.9 cm^{-1} bands are due to a Ti−η^2-$(C_2H_2)_2$ complex. Our calculations reveal blue shifts from the Ti−η^2-(C_2H_2) complex modes. The 1446.3 cm^{-1} band is probably due to a higher complex. On the other hand, the 1441.4 cm^{-1} band shows no carbon-13 shift and the same H/D ratio as HC≡C−TiH, which points to a higher (HC≡C−TiH)(C_2H_2) complex.

The Ti vinylidene product is not identified in this study. The vinylidene complex (Ti=CCH_2) would show its strong C−C stretching and CH_2 wagging absorptions at about 1514 and 843 cm^{-1}, which are not observed in these Ti + C_2H_2 spectra. Unlike in the Ni and Pt systems,[3,4] where the vinylidene product is one of the primary products with lowest energy, Ti=CCH_2(T, for triplet state) is less stable (18 kcal/mole lower in energy than the reactants) in this Ti + C_2H_2 system than HC≡C−TiH(T) and Ti−η^2-(C_2H_2)(T) (35 and 45 kcal/mol lower in energy than the reactants).

Zr + C_2H_2. Figures 3 and 4 show the Zr + C_2H_2 and Zr + C_2D_2 spectra in the product absorption regions, which are similar to the Ti spectra shown in Figures 1 and 2, and Table 4 lists the observed frequencies. Two sets of product absorptions marked **i** and $\boldsymbol{\pi}$ are observed. The **i** absorptions increase about 20 and 70% upon visible and UV photolysis, whereas the $\boldsymbol{\pi}$ absorptions remain unchanged upon visible photolysis but decrease about 50% upon UV photolysis (Figures 3a–d and 4a−d). Similar to the Ti case, the present result suggests that the product responsible for the $\boldsymbol{\pi}$ absorptions converts to the product corresponding to the **i** absorptions upon UV photolysis.

TABLE 4: Frequencies of Product Absorptions Observed from Reactions of Zr with Acetylene Isotopomers in Excess Argon[a]

	C_2H_2	C_2D_2	$^{13}C_2H_2$	description
π	2993.2	2294.9	2982.3	A_1 C−H str.
	2966.2	2247.3	2957.3	B_2 C−H str.
	1316.9	1282.0	1277.8	A_1 C−C str.
	1061.7, 1053.7	911.7, **907.1**	1043.1, 1033.0	B_2 HCCH bend
	633.7	467.0	630.3	B_1 HCCH bend
	588.6	482.0	574.1	B_2 ZrC_2 str.
	541.3	525.5	525.5	A_1 ZrC_2 str.
i	1959.5, 1955.1	1846.5, 1841.7	1889.6, 1885.2	A′ C−C str.
	1557.7, 1549.7, **1541.9**, 1531.7	1116.8, 1111.4, **1106.2**, 1101.2	1558.3, 1549.4, **1541.9**, 1534.5	A′ C−C str.
	636.3			A″ CCH bend
	446.2, 440.9		435	A′ C−Zr str.

[a] All frequencies are in cm^{-1}. Stronger absorptions are bold. Description gives the major coordinate, and ***π*** and **i** stand for the π and insertion products, respectively.

The strongest **i** absorptions are observed at 1557.7, 1549.7, 1541.9, and 1531.7 cm^{-1}, split by the matrix, among which the one at 1541.9 cm^{-1} is the strongest until the end of photolysis. However, they later all merge to the absorption at 1531.7 cm^{-1} in the process of annealing. They show essentially no ^{13}C shifts but D shifts of about 436 cm^{-1} (H/D shift of 1.393), and their frequencies are compared to the ZrH_2 and ZrD_2 frequencies of 1518.6 and 1092.5 cm^{-1}.[18] These Zr−H stretching absorptions show that oxidative C−H insertion of acetylene also readily occurs by Zr atoms. Another **i** absorption is observed at 446.2 cm^{-1}, and its ^{13}C counterparts are observed at 435 cm^{-1}. It is assigned to the C−Zr stretching mode of HC≡C−ZrH on the basis of the frequency without observation of the D counterpart, which is essentially outside of our observation limit.

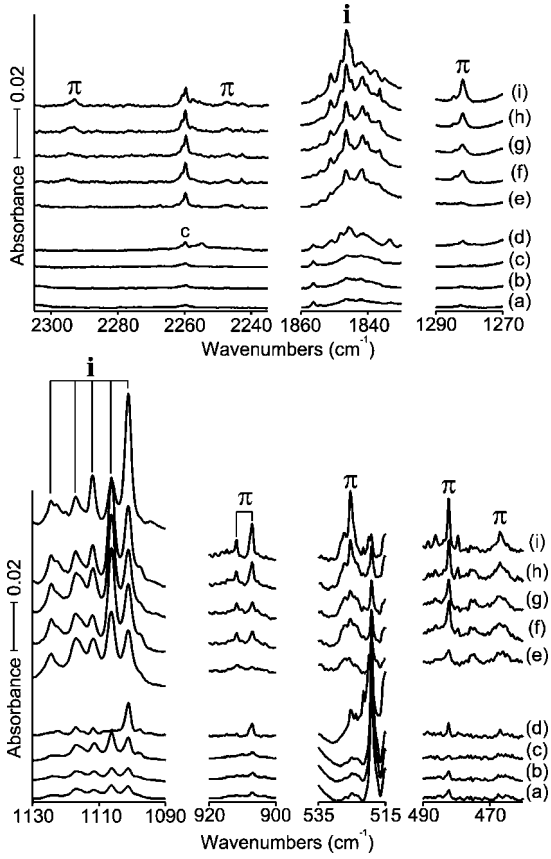

Figure 4. IR spectra in the product absorption regions for laser-ablated Zr atoms codeposited with C_2D_2 in excess argon at 8 K and their variation. (a) Zr + 0.5% C_2D_2 in Ar codeposited for 1 h. (b) As that in (a) after photolysis ($\lambda > 420$ nm). (c) As that in (b) after photolysis ($240 < \lambda < 380$ nm). (d) As that in (c) after annealing to 36 K. (e) Zr + 0.25% C_2D_2 in Ar codeposited for 1.5 h. A laser power three times as high is used. (f) As that in (e) after annealing to 24 K. (g) As that in (e) after 45 min photolysis ($\lambda < 220$ nm). (h) As that in (g) after annealing to 28 K. (i) As that in (h) after annealing to 34 K. Here, **i** and ***π*** denote the product absorption group.

The **i** absorptions at 1959.5 and 1955.1 cm^{-1} have their D counterparts at 1846.5 and 1841.7 and ^{13}C counterparts at 1889.6 and 1885.2 cm^{-1} (H/D and 12/13 ratios of 1.061 and 1.037). They are assigned to the C−C stretching mode on the basis of the high frequency and the considerable ^{13}C shift. A weak **i** absorption is observed at 636.3 cm^{-1} (not shown) and tentatively assigned to the A″ CCH bending mode of HC≡C−ZrH. As shown in Table 5, the observed absorptions correspond to the bands predicted to be strong for the insertion complex, and the frequencies are consistent with the predicted values. The good agreements between the observed and predicted vibrational characteristics support formation of the ethynyl Zr hydride complex.

In order to better observe the ***π*** absorptions, a separate trial, similar to the Ti case, was carried out with a laser power three times as high and with a procedure of deposition, annealing, full arc photolysis, and annealing at higher temperatures (Figures 3e–i and 4e−i). The ***π*** absorptions grow fast in the initial annealing to 24 K but decrease to about half upon the following full arc photolysis. They recover and further increase in the following annealing at higher temperatures. The observed π frequencies are compared with the DFT frequencies in Table 6, showing that 7 out of the 8 IR-active bands are observed. The unobserved A_1 HCCH bending band is predicted to be too weak to observe (1 km/mol). The observed frequencies are also consistent with the calculated values. The observed frequencies mostly range within 0.95−0.98 of the B3LYP values, as shown in Table 6. The C−C stretching frequency of 1316.7 cm^{-1} is even lower than that of Ti−η^2-(C_2H_2), indicating that the back-donation to the C−C antibonding orbital, which weakens the C−C bond, is even stronger than that in Ti π complex.

Parallel to the Ti case, the insertion and π complexes are more stable than the vinylidene complex in this Zr + C_2H_2 system; HC≡C−ZrH, Zr−η^2-(C_2H_2), and Zr=CCH_2 are 47, 59, and 31 kcal/mol lower in energy than the reactants. The vinylidene product, which would show the strong C−C stretching and CH_2 wagging bands at about 1470 and 814 cm^{-1}, is not identified in the Zr + C_2H_2 spectra.

Hf + C_2H_2. Figures 5 and 6 show the Hf + C_2H_2 and Hf + C_2D_2 spectra and their variations in the product absorption regions. Similar to the Ti and Zr cases, two sets of product absorptions marked **i** and ***π*** are observed. The **i** absorptions increase 10 and 25% upon visible and UV photolysis and

TABLE 5: Calculated Fundamental Frequencies of HC≡C−ZrH Isotopomers in the Ground $^3A''$ Electronic State[a]

	HC≡C−ZrH				DC≡C−ZrD				$H^{13}C{\equiv}{}^{13}C$−ZrH			
approximate description	obs	BPW91	B3LYP	int.	obs	BPW91	B3LYP	int.	obs	BPW91	B3LYP	int
A′ C−H str.	covered	3372.4	3438.0	37	covered	2590.1	2649.8	8	covered	3355.6	3420.6	38
A′ C−C str.	1955.9	1949.1	2029.4	39	1841.7	1834.2	1903.1	54	1885.2	1878.7	1956.3	35
A′ Zr−H str.	1541.9	1608.9	1618.9	427	1106.2	1144.6	1151.8	219	1541.9	1608.9	1618.9	427
A′ CCH bend		673.4	712.1	37		534.2	565.3	16		667.0	705.2	38
A′ C−Zr str.	446.2	468.7	464.6	162		424.6	424.0	102	435	462.6	458.1	156
A′ CZrH bend		382.9	379.7	5		310.5	306.5	19		375.1	372.3	5
A′ CCZr bend		147.0	148.1	14		131.9	132.4	12		142.6	143.7	13
A″ CCH bend	636.3	659.0	710.8	35		522.7	563.9	14		652.6	703.8	36
A″ CCZr bend		160.0	158.6	16		148.4	147.3	19		154.9	153.4	14

[a] Frequencies and intensities are computed with 6-311++G(3df, 3pd) for harmonic calculations, and the SDD core potential and basis set are used for Zr. Frequencies and intensities are in cm^{-1} and km/mol, and intensities are calculated with B3LYP. The symmetry notations are based on the C_s structure.

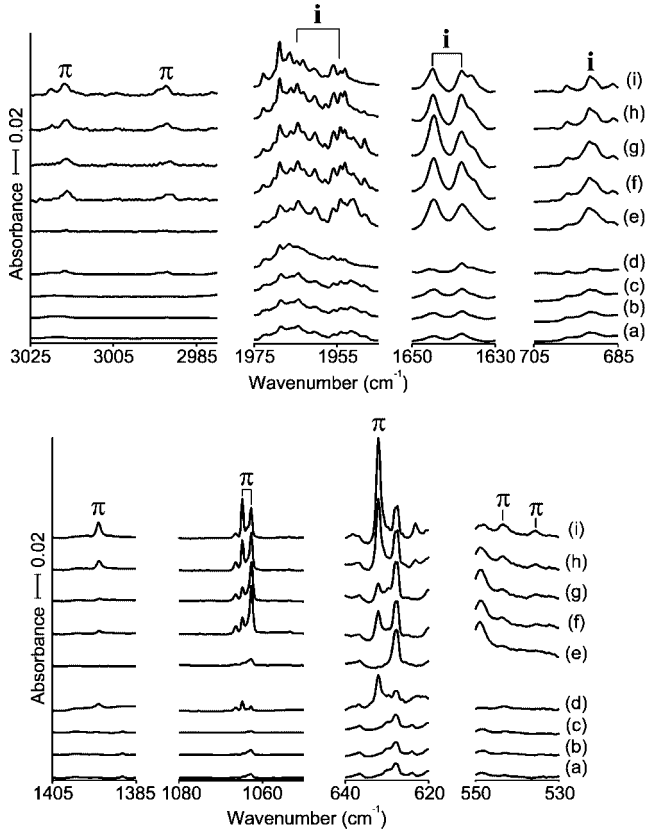

Figure 5. IR spectra in the product absorptions regions for laser-ablated Hf atoms codeposited with C_2H_2 in excess argon at 8 K and their variation. (a) Hf + 0.5% C_2H_2 in Ar codeposited for 1 h. (b) As that in (a) after photolysis ($\lambda > 420$ nm). (c) As that in (b) after photolysis ($240 < \lambda < 380$ nm). (d) As that in (c) after annealing to 36 K. (e) Hf + 0.25% C_2H_2 in Ar codeposited for 1.5 h. A laser power three times as high is used. (f) As that in (e) after annealing to 25 K. (g) As that in (f) after 60 min photolysis ($\lambda < 220$ nm). (h) As that in (g) after annealing to 29 K. (i) As that in (h) after annealing to 35 K. Here, **i** and $\boldsymbol{\pi}$ denote the product absorption group.

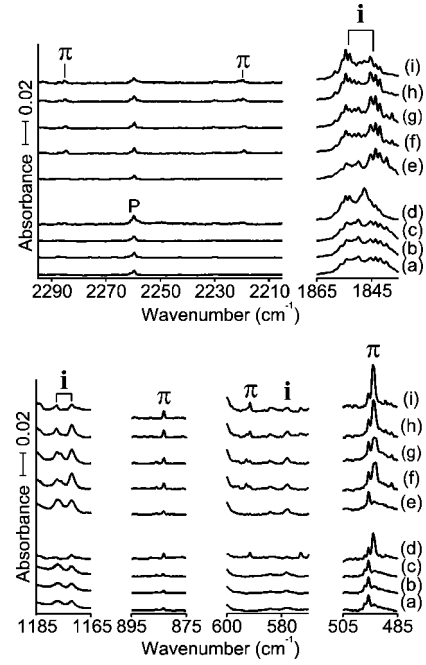

Figure 6. IR spectra in the product absorptions regions for laser-ablated Hf atoms codeposited with C_2D_2 in excess argon at 8 K and their variation. (a) Hf + 0.5% C_2D_2 in Ar codeposited for 1 h. (b) As that in (a) after photolysis ($\lambda > 420$ nm). (c) As that in (b) after photolysis ($240 < \lambda < 380$ nm). (d) As that in (c) after annealing to 36 K. (e) Hf + 0.25% C_2D_2 in Ar codeposited for 1 h. A laser power three times as high is used. (f) As that in (e) after annealing to 26 K. (g) As that in (f) after 30 min photolysis ($\lambda < 220$ nm). (h) As that in (g) after annealing to 21 K. (i) As that in (h) after annealing to 37 K. Here, **i** and $\boldsymbol{\pi}$ denote the product absorption group.

gradually decrease upon annealing. The $\boldsymbol{\pi}$ absorptions remain unchanged upon visible irradiation but decrease about 50% upon UV photolysis, but they recover and further increase upon annealing at higher temperatures. The $\boldsymbol{\pi}$ absorptions are more apparent in the spectra, with a higher laser energy owing to increased Hf atom concentration (Figures 5e–i and 6e−i), particularly after initial annealing (f−i). The observed frequencies are summarized in Table 7 and compared with the DFT frequencies in Tables 8 and 9.

The strong **i** absorptions split by the matrix are observed at 1645.1 and 1638.0 cm^{-1}, and they show essentially no ^{13}C shifts and D shifts of 467.9 and 466.0 cm^{-1} (H/D ratios of 1.397 and 1.398). The frequencies are compared with the HfH_2 frequencies of 1629.1 and 1622.4 cm^{-1} and HfD_2 frequencies of 1166.7 and 1161.0 cm^{-1}.[18] Parallel to the Ti and Zr cases, the Hf−H stretching absorptions strongly suggest that oxidative C−H insertion readily occurs to form ethynyl hafnium hydride (HC≡C−HfH). The weak **i** absorption at 697.1 cm^{-1} has its D and ^{13}C counterparts at 578.2 and 685.1 cm^{-1} (H/D and 12/13 ratios of 1.206 and 1.018) and is assigned to the A″ CCH bending mode on the basis of the frequency and the substantial D shift. A weak **i** absorption at 460.1 cm^{-1} has its ^{13}C counterpart at 441.0 cm^{-1}, but the D counterpart is not observed due to its low frequency essentially outside of our observation limit. It is assigned to the C−Hf stretching mode. The broad **i** absorptions at 1964.4 and 1954.1 cm^{-1} have the D counterpart at 1854.3 and 1845.2 cm^{-1} (H/D ratios of both 1.059) and the

TABLE 6: Calculated Fundamental Frequencies of Zr(C_2H_2) Isotopomers in the Ground $^3A_2$ Electronic State[a]

	Zr(C_2H_2)				Zr(C_2D_2)				Zr($^{13}C_2H_2$)			
approximate description	obs	BPW91	B3LYP	int.	obs	BPW91	B3LYP	int.	obs	BPW91	B3LYP	int.
A_1 C−H str.	2993.2	3088.8	3149.4	23	2294.9	2305.4	2351.8	5	2982.3	3077.3	3137.5	24
A_1 C−C str.	1316.9	1365.8	1424.6	17	1282.0	1316.6	1373.5	17	1277.8	1315.8	1372.3	16
A_1 HCCH bend		779.5	815.0	1		571.2	595.5	1		778.6	814.0	1
A_1 ZrC_2 str.	541.3	550.3	554.6	11	525.5	526.8	532.1	10	525.5	534.2	538.6	10
A_2 HCCH bend		885.2	935.2	0		703.9	743.8	0		876.1	925.6	0
B_1 HCCH bend	633.7	628.8	654.9	64	467.0	476.3	495.9	42	630.3	625.3	651.3	63
B_2 C−H str.	2966.2	3062.2	3122.4	11	2247.3	2251.5	2295.4	4	2957.3	3053.1	3113.1	11
B_2 HCCH bend	1061.7	1042.1	1086.1	30	907.1	896.1	927.7	11	1043.1	1023.8	1067.7	30
B_2 ZrC_2 str.	588.6	576.0	569.3	28	482.0	492.6	489.9	28	574.1	562.1	555.2	26

[a] Frequencies and intensities are computed with 6-311++G(3df, 3pd) for harmonic calculations, and the SDD core potential and basis set are used for Zr. Frequencies and intensities are in cm^{-1} and km/mol, and intensities are calculated with B3LYP. The symmetry notations are based on the C_{2v} structure.

TABLE 7: Frequencies of Product Absorptions Observed from Reactions of Hf with Acetylene Isotopomers with Excess Argon[a]

	C_2H_2	C_2D_2	$^{13}C_2H_2$	CHCD	description
π	3016.3	2284.9	3004.0	3004.5	A_1 C−H str.
	2992.0	2219.4	2983.0	2248.6	B_2 C−H str.
	1393.9		1342.1		A_1 C−C str.
	1062.6	883.1	1044.2	1003.8	B_2 HCCH bend
		592.9			A_1 HCCH bend
	632.2	493.4	627.5	563.7	B_1 HCCH bend
	543.5	453.3	527.3		B_2 HfC_2 str.
	535.5	covered[b]	512.4		A_1 HfC_2 str.
i	1964.4, 1954.1	1854.3, 1845.2	1894.1, 1885.8		A′ C−C str.
	1645.1, **1638.0**	1177.2, **1172.0**	1644.7, **1638.0**	1645.1, **1638.0**, 1177.2, **1172.0**	A′ Hf−H str.
	697.1	578.2	685.1		A″ CCH bend
	460.1		441.0		A′ C−Hf str.

[a] All frequencies are in cm^{-1}. Stronger absorptions are bold. Description gives the major coordinate; π and **i** stand for the π and insertion products, respectively. [b] Overlapped by precursor absorption.

TABLE 8: Calculated Fundamental Frequencies of HC≡C−HfH Isotopomers in the Ground $^1A'$ Electronic States[a]

	HC≡C−HfH				DC≡C−HfD				H^{13}C≡^{13}C−HfH			
approximate description	obs	BPW91	B3LYP	int.	obs	BPW91	B3LYP	int.	obs	BPW91	B3LYP	int.
A′ C−H str.		3372.4	3437.7	38		2593.9	2652.0	5		3355.5	3420.1	40
A′ C−C str.	1964.4	1968.0	2040.0	62	1854.3	1850.0	1911.8	78	1894.1	1896.9	1966.5	55
A′ Hf−H str.	1638.0	1660.6	1692.0	349	1172.0	1178.0	1200.3	176	1638.0	1660.6	1692.0	350
A′ CCH bend		661.7	712.7	36		527.1	568.0	17		655.2	705.6	36
A′ C−Hf str.	460.1	485.8	481.2	46		419.7	421.0	58	441.0	481.4	476.2	41
A′ CHfH bend		402.6	395.7	23		344.6	333.3	2		390.9	384.9	24
A′ CCHf bend		154.2	159.6	7		136.0	147.1	6		149.7	154.9	7
A″ CCH bend	697.1	717.0	751.4	30	578.2	571.2	598.5	12	685.1	709.7	743.8	31
A″ CCHf bend		152.1	159.0	10		141.3	141.2	10		147.2	153.9	9

[a] Frequencies and intensities are computed with 6-311++G(3df, 3pd) for harmonic calculations, and the SDD core potential and basis set are used for Hf. Frequencies and intensities are in cm^{-1} and km/mol, and intensities are calculated with B3LYP. The symmetry notations are based on the C_s structure.

^{13}C counterparts at 1894.1 and 1885.8 cm^{-1} (12/13 ratios of 1.037 and 1.036). They are assigned to the C−C stretching mode on the basis of the frequency and the sizable ^{13}C shift.

Table 9 shows that the vibrational bands of the hafnium−acetylene π complex with non-negligible intensities are all observed, except for the IR-inactive and very weak A_2 and A_1 HCCH bending modes. The observed frequencies are all in the range of 0.92−0.98 of the DFT values, as shown in Table 9, and the consistency substantiates formation of the π complex. While the C−C stretching frequency of 1393.9 cm^{-1} is still much lower than those of the previously studied Ni and Pt π complexes, it is the highest among those of the group 4 metal π complexes. This suggests that the back-donation of the dπ electron from the Hf atom to the antibonding π^* orbital of C_2H_2 is weaker than those from the Ti and Zr atoms.

Unlike the Ti and Zr cases, the Hf vinylidene complex is almost as stable as the insertion complex, and the hafnium

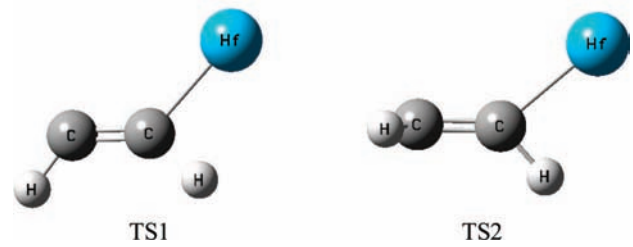

Figure 7. The transition-state structures from the Hf−η^2-(C_2H_2) complex to HC≡C−HfH (TS1) and to Hf═CCH_2 (TS2) on the singlet potential surface. TS1 is 21 kcal/mol more stable than TS2, which is consistent with the observation that only the insertion product is identified in the matrix spectra.

products are all singlet ground states. The HC≡C−HfH(S), Hf−η^2-(C_2H_2)(S), and Hf═CCH_2(S) are 44, 58, and 43 kcal/mole lower in energy than the reactants. However, the vinylidene

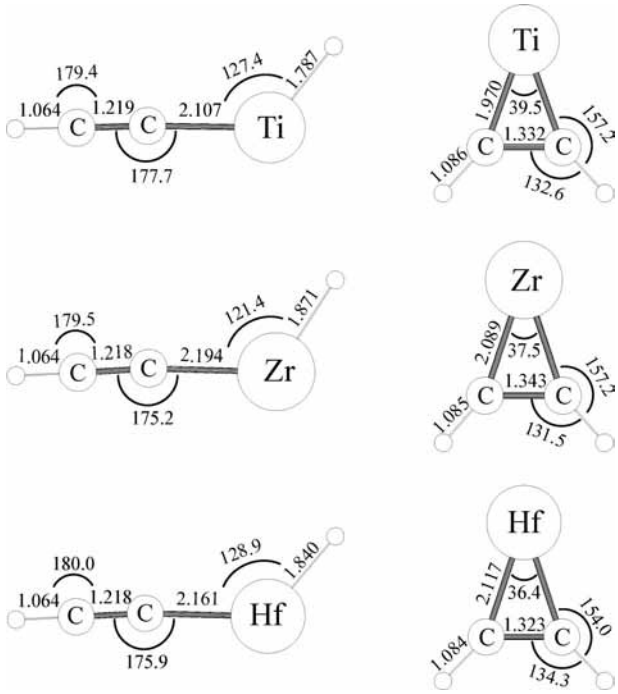

Figure 8. The optimized molecular structures of the identified acetylene insertion and π complexes of the group 4 transition metals. The structures are calculated with B3LYP/6-311++G(3df,3pd), and the SDD core potential and basis set are used for Zr and Hf. The insertion complexes (HC≡C−TiH(T), HC≡C−ZrH(T), and HC≡C−HfH(S)) all have a C_s structure, whereas the π complexes (Ti−C_2H_2(T), Zr−C_2H_2(T), and Hf−C_2H_2(S)) have a C_{2v} structure. Notice that the carbon−metal bonds of the π complexes are shorter than those of the insertion products. The bond lengths and angles are in Å and degrees.

complex, which would show strong absorptions at around 2924, 1600, and 945 cm^{-1}, is not identified in the matrix IR spectra. This suggests that in this Hf system, the oxidative C−H insertion is more favored than the hydrogen migration, which is required for formation of the vinylidene complex. DFT calculations are performed for the transition states between HC≡C−HfH(S) and Hf−η^2-(C_2H_2)(S) and between the Hf═CCH_2(S) and Hf−η^2-(C_2H_2)(S) on the basis of the assumption that the π complex is formed first and rearrangement to the products follows. The transition state to the insertion product is 21 kcal/mol lower in energy than the transition state to the vinylidene complex, which is consistent with the present result. The transition-state structures are shown in Figure 7.

Structures of HC≡C−MH and M−η^2-(C_2H_2). The optimized structures of group 4 metal insertion and π complexes are illustrated in Figure 8. The ethynyl complexes all have planar (C_s) structures ($^3A'$ for Ti and Zr, $^1A'$ for Hf), whereas the π complexes have C_{2v} structures ($^3A_2$ for Ti and Zr, $^1A_1$ for Hf). The C−Ti bond lengths of HC≡C−TiH(T) and Ti−η^2-(C_2H_2)(T) of 2.107 and 1.970 Å are compared with that of 2.058 Å measured for $(CH_3)_2TiCl_2$.[19] Clearly, Ti−η^2-(C_2H_2) is a strong π complex such that its C−Ti and C−C bonds are shorter and longer than those of HC≡C−TiH. They are also consistent with the measured unusually high C−Ti (594.5 and 573.0 cm^{-1}) and low C−C (1364.6 cm^{-1}) stretching frequencies of the π complex. They are, for example, compared with the C−Ni stretching frequencies of 548.6, 545.3, and 539.6 cm^{-1} and the C−C stretching frequencies of 1647.4 cm^{-1} measured from another first-row transition-metal−acetylene complex, Ni−η^2-(C_2H_2).[3] Figure 8 also shows that the Zr and Hf π complexes also show the shorter C−M and longer C−C bonds than those

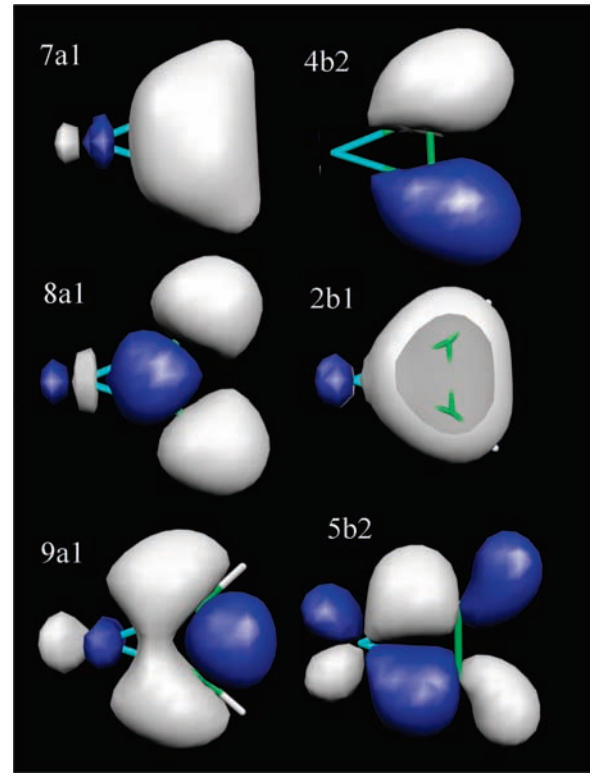

Figure 9. The doubly occupied valence orbitals in Ti−η^2-(C_2H_2) computed using the B3LYP density functional and drawn with Molekel. [Flükiger, P.; Lüthi, H. P.; Portmann, S.; Weber, J. MOLEKEL 4.0; : Manno, Switzerland, 2000].

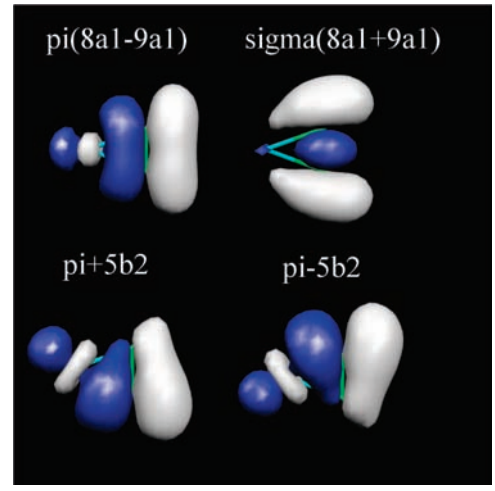

Figure 10. Localized orbitals in Ti−η^2-(C_2H_2) computed and drawn as in previous figure.

of the ethynyl complexes. The longer C−C bonds are consistent with the observed high C−M stretching (541.3 and 588.6 cm^{-1} for Zr−η^2-(C_2H_2) and 535.5 and 543.5 cm^{-1} for Hf−η^2-(C_2H_2)) and unusually low C−C stretching frequencies (1316.7 and 1393.9 cm^{-1}, respectively).

On the basis of the observed frequencies, it is clear that the group 4 metals form stronger π complexes than the group 8 metals. Given the smaller electronegativites and fewer d electrons, one might have expected the group 4 to be more weakly bound. An inspection of the Mulliken populations shows that bonding in Ti−η^2-(C_2H_2) is derived from the Ti excited $3d^34s^1$ occupation. The open-shell orbitals are a Ti 3dδ(a_2) orbital that has a weak interaction with the C_2H_2 out-of-plane π^* orbital and a Ti nonbonding sd hybrid orbital. The doubly

TABLE 9: Calculated Fundamental Frequencies of Hf(C_2H_2) Isotopomers in the Ground $^1A_1$ States[a]

	Hf(C_2H_2)				Hf(C_2D_2)				Hf($^{13}C_2H_2$)				Hf(CHCD)			
approximate description	obs	BPW91	B3LYP	int.	obs	BPW91	B3LYP	int.	obs	BPW91	B3LYP	int.	obs	BPW91	B3LYP	int.
A_1 C−H str.	3016.3	3090.8	3157.9	22	2284.9	2317.3	2367.4	7	3004.0	3078.6	3145.5	22	3004.5	3076.7	3144.1	17
A_1 C−C str.	1393.9	1481.7	1516.3	2		1423.4	1456.8	3	1343.1	1427.3	1460.6	2		1452.1	1486.1	3
A_1 HCCH bend		820.7	847.6	0	592.9	606.0	622.9	5		819.4	846.2	0		697.1	717.5	1
A_1 HfC_2 str.	535.5	548.2	553.5	16	covered	518.3	525.8	11	512.4	530.7	535.8	15		547.4	552.4	15
A_2 HCCH bend		944.7	978.9	0		755.6	782.8	0		934.5	968.4	0		875.0	906.4	5
B_1 HCCH bend	632.2	651.6	673.3	41	493.4	492.3	508.5	25	627.5	648.1	669.7	41	563.7	547.3	565.6	28
B_2 C−H str.	2992.0	3061.9	3129.5	13	2219.4	2249.4	2299.2	7	2983.0	3052.9	3120.4	13	2248.6	2283.8	2333.8	7
B_2 HCCH bend	1062.6	1044.7	1089.0	39	883.1	892.8	926.9	21	1044.2	1027.2	1071.1	39	1003.8	993.6	1034.0	30
B_2 HfC_2 str.	543.5	551.6	554.5	7	453.3	473.5	477.8	8	527.3	537.6	540.3	6		489.8	495.1	8

[a] Frequencies and intensities are computed with 6-311++G(3df, 3pd) for harmonic calculations, and the SDD core potential and basis set are used for Hf. Frequencies and intensities are in cm^{-1} and km/mol, and intensities are calculated with B3LYP. The symmetry notations are based on the C_s structure.

occupied valence orbitals are plotted in Figure 9. The character of some of the orbitals is obvious from the plots. The $4b_2$ orbital is essentially the antisymmetric combination of the C−H σ bonds, while the $2b_1$ is the C_2H_2 out-of-plane π orbital, which shows some donation of charge to the empty Ti out-of-plane $3d\pi$ orbital. The $5b_1$ orbital shows a bond between the Ti in-plane $3d\pi$ orbital and the C_2H_2 in-plane π^* orbital. The $7a_1$ is the totally symmetric combination of the C−C σ bond and the two C−H σ bonds. While the character of the $7a_1$, $4b_2$, $2b_1$, and $5b_2$ orbitals seems clear, the $8a_1$ and $9a_1$ orbitals appear somewhat odd. In Figure 10, we show the symmetric and antisymmetric combinations of these two orbitals, which appear much more like a σ and a π orbital than the original delocalized orbitals. It is now clear that the π orbital forms a bond between the Ti and C_2H_2. Adding and subtracting the bonding $5b_2$ orbital with the bonding π orbital clearly shows the two Ti−C bonds; see Figure 10. Thus, it is the formation of two Ti−C bonds in the group 4 systems than leads to the stronger bonding than that in the group 8 systems. While bonds form, the Ti atom is weakly bound to the C_2H_2, and we still refer to it as a π complex.

The bonding in Zr−η^2-(C_2H_2) is similar to that in Ti−η^2-(C_2H_2), while Hf−η^2-(C_2H_2) shows some differences, namely, the Hf is in the $5d^26s^2$ occupation and does not need to promote to the d^3s^1 occupation like the lighter group 4 metals. This change is due to relativistic effects that stabilize the 6s orbital, making the promotion more costly. The relativistic contraction of the 6s orbital also means that the 5d and 6s orbitals are more similar in size than the analogous orbitals for Ti and Zr. Therefore, Hf can form bonds similar to those in Ti and Zr in the metal−η^2-(C_2H_2) complexes without promoting to the excited state. Thus, Hf has a doubly occupied sd hybrid orbital instead of two open-shell orbitals. This change in the bonding coupled with the poorer overlap of the diffuse 5d orbital with C_2H_2 in-plane π orbitals most likely results in the weaker Hf bonding, as observed in the C−C stretching frequencies of the Ti, Zr, and Hf π complexes that are 1364.6, 1316.7, and 1393.9 cm^{-1}, respectively. Because the 6s relativistic stabilization actually weakens the Hf bonding, which is mostly d in character, the carbon−metal bond length in the π complex does not show a decrease with Hf as normally expected with lanthanide contraction (1.970, 2.089, and 2.177 Å for the Ti, Zr, and Hf π complexes, respectively). In contrast the $H_2Ti-C_2H_2$ complex has a higher 1465 cm^{-1} C−C stretching frequency.[16]

The M−H bond lengths of the ethynyl Ti, Zr, and Hf hydride complexes are 1.787, 1.871, and 1.840 Å, the C−M bond lengths are 2.107, 2.194, and 2.161 Å, and the C−M−H bond angle (∠CMH) are 127.4, 121.4, and 128.9°, respectively. The short bonds and the large bond angle of the Hf complex recall relativistic effects.[20] These trends are also consistent with the observed C−M stretching frequencies of 452.6, 446.2, and 460.1 cm^{-1} when going down the column.

We consider both the singlet and triplet states of the HC_2MH and M−C_2H_2 structures. The ground-state results are reported in the article, while the excited-state results are given in the Supporting Information. For the Ti- and Zr-containing species, the triplet states are lower using both the B3LYP and BPW91 approaches. (Note that for $HTiC_2H$, we considered both a closed shell and $M_s = 0$ (which is a mixture of singlet and triplet states) treatments of the singlet state, and both treatments yielded a triplet ground state). While the computed IR spectra of the singlet and triplet states are similar, the triplet states appear to be in better agreement with the experimental observations. On this basis, we conclude that the Ti and Zr species have triplet ground states. For the Hf species, the triplet and singlet states

are much closer in energy. We report the singlet results, which are the ground states at the B3LYP level, and their computed spectra agree better with experiment. However, we should note that the triplet and singlet IR spectra for the Hf compounds show much smaller differences than do the singlet and triplet states for the Ti and Zr species. Thus while, we tentatively identify the Hf ground states as singlets, we cannot completely rule out the triplets.

Conclusions

The insertion and π complexes (HC≡C−MH and M−η^2-(C_2H_2)) are the primary products of the reactions of laser-ablated Ti, Zr, and Hf atoms with acetylene. On the other hand, the vinylidene product (M═C═CH_2) is not identified in the matrix IR spectra, most probably due to its relatively high energy and more unstable transition state. The strong M−H, C−M, and C−C stretching absorptions of the ethynyl product are clearly visible in the original deposition spectra and increase upon photolysis, whereas a higher laser power and initial annealing are needed for better observation of the π absorptions. The absorptions from the π complex decrease upon UV photolysis, while those from the insertion complex increase, suggesting that the π complex converts to the C−H insertion product with the photon energy.

The C−M and M−H bond lengths of the ethynyl complex (HC≡C−MH) decrease with going from Zr to Hf, and its C−M stretching frequency increases, which is more evidence of the lanthanide contraction. The C−C stretching frequencies of M−η^2-(C_2H_2) are unusually low, revealing that group 4 metals are forming exceptionally strong π complexes. Since the metal−C_2H_2 bonding is mostly d in character, the relativistic stabilization of the Hf 6s orbital reduces the magnitude of metal interaction. This results in the C−C stretching frequency of the π complex to first decrease and then increase with going from Ti to Zr and to Hf and in C−M bond distances that continuously increase in the π complex when going down the column.

Supporting Information Available: Six tables of calculated frequencies for higher-energy product states. This material is available free of charge via the Internet at http://pubs.acs.org.

Acknowledgment. We gratefully acknowledge financial support from NSF Grant CHE 03-52487 to L.A. and use of the computing system of the KISTI Supercomputing Center. The thermal Ti experiment performed by L. Manceron is also greatly appreciated.

References and Notes

(1) (a) Bowden, F. L.; Lever, A. B. P. *Organomet. Chem. Rev.* **1968**, *3*, 227. (b) Crabtree, R. H. *The Organometallic Chemistry of the Transition Metals*; Wiley: New York, 2001, p 190.

(2) (a) Kasai, P. H. *J. Am. Chem. Soc.* **1983**, *105*, 6704. (b) Kasai, P. H. *J. Am. Chem. Soc.* **1982**, *104*, 1165. (c) Kasai, P. H.; McLeod, D., Jr.; Watanabe, T. *J. Am. Chem. Soc.* **1980**, *102*, 179. (d) Ozin, G. A.; McIntosh, D. F.; Power, W. J.; Messmer, R. P. *Inorg. Chem.* **1981**, *20*, 1782. (e) Chenier, J. H. B.; Howard, J. A.; Mile, B.; Sutcliffe, R. *J. Am. Chem. Soc.* **1983**, *105*, 788. (f) Kasai, P. H. *J. Phys. Chem.* **1982**, *86*, 4092.

(3) (a) Kline, E. S.; Kafafi, Z. H.; Hauge, R. H.; Margrave, J. L. *J. Am. Chem. Soc.* **1985**, *107*, 7559. (Fe + C_2H_2). (b) Kline, E. S.; Kafafi, Z. H.; Hauge, R. H.; Margrave, J. L. *J. Am. Chem. Soc.* **1987**, *109*, 2402. (Ni + C_2H_2)

(4) (a) Huang, Z.; Zeng, A.; Dong, J.; Zhou, M. *J. Phys. Chem. A* **2003**, *107*, 2329. (Cr + C_2H_2). (b) Wang, X.; Andrews, L. *J. Phys. Chem. A* **2003**, *107*, 337. (Pd + C_2H_2). (c) Wang, X.; Andrews, L. *J. Phys. Chem. A* **2004**, *108*, 4838. (Pt + C_2H_2)

(5) Manceron, L.; Andrews, L. *J. Am. Chem. Soc.* **1985**, *107*, 563. (Li + C_2H_2)

(6) (a) Siegbahn, P. E. M. *Theor. Chim. Acta* **1994**, *87*, 277. (b) Sodupe, M.; Bauschlicher, C. W., Jr *J. Phys. Chem* **1991**, *95*, 8640. (c) Martinez, M.; Michelini, M.; Del, C.; Rivalta, I.; Russo, N.; Sicilia, E. *Inorg. Chem.* **2005**, *44*, 9807.

(7) Porembski, M.; Weisshaar, J. C. *J. Phys. Chem. A* **2000**, *104*, 1524, and references therein.

(8) (a) Dewar, M. J. *Bull. Soc. Chim. Fr.* **1951**, *18*, C71. (b) Chatt, J.; Duncanson, L. A. *J. Chem. Soc.* **1953**, 2939.

(9) (a) Thompson, C. A.; Andrews, L. *J. Am. Chem. Soc.* **1996**, *118*, 10242. (Be + C_2H_2). (b) Andrews, L.; Hassanzadeh, P.; Martin, J. M. L.; Taylor, P. R. *J. Phys. Chem.* **1993**, *97*, 5839. (B + C_2H_2). (c) Chertihin, G. V.; Andrews, L.; Taylor, P. R. *J. Am. Chem. Soc.* **1994**, *116*, 3513. (Al + C_2H_2). (d) Andrews, L.; Kushto, G. P.; Marsden, C. J. *Chem.—Eur. J.* **2006**, *12*, 8324. (Th, U + C_2H_2)

(10) (a) Andrews, L.; Citra, A. *Chem. Rev.* **2002**, *102*, 885, and references therein. (b) Andrews, L. *Chem. Soc. Rev.* **2004**, *33*, 123, and references therein.

(11) Kudin, K. N.; Burant, J. C.; Millam, J. M.; Iyengar, S. S.; Tomasi, J.; Barone, V.; Mennucci, B.; Cossi, M.; Scalmani, G.; Rega, N.; Petersson, G. A.; Nakatsuji, H.; Hada, M.; Ehara, M.; Toyota, K.; Fukuda, R.; Hasegawa, J.; Ishida, M.; Nakajima, T.; Honda, Y.; Kitao, O.; Nakai, H.; Klene, M.; Li, X.; Knox, J. E.; Hratchian, H. P.; Cross, J. B.; Adamo, C.; Jaramillo, J.; Gomperts, R.; Stratmann, R. E.; Yazyev, O.; Austin, A. J.; Cammi, R.; Pomelli, C.; Ochterski, J. W.; Ayala, P. Y.; Morokuma, K.; Voth, G. A.; Salvador, P.; Dannenberg, J. J.; Zakrzewski, V. G.; Dapprich, S.; Daniels, A. D.; Strain, M. C.; Farkas, O.; Malick, D. K.; Rabuck, A. D.; Raghavachari, K.; Foresman, J. B.; Ortiz, J. V.; Cui, Q.; Baboul, A. G.; Clifford, S.; Cioslowski, J.; Stefanov, B. B.; Liu, G.; Liashenko, A.; Piskorz, P.; Komaromi, I.; Martin, R. L.; Fox, D. J.; Keith, T.; Al-Laham, M. A.; Peng, C. Y.; Nanayakkara, A.; Challacombe, M.; Gill, P. M. W.; Johnson, B.; Chen, W.; Wong, M. W.; Gonzalez, C.; Pople, J. A. *Gaussian 03*, revision B.04; Gaussian, Inc.: Pittsburgh, PA, 2003.

(12) (a) Becke, A. D. *J. Chem. Phys.* **1993**, *98*, 5648. (b) Lee, C.; Yang, Y.; Parr, R. G. *Phys. Rev. B* **1988**, *37*, 785.

(13) Andrae, D.; Haeussermann, U.; Dolg, M.; Stoll, H.; Preuss, H. *Theor. Chim. Acta* **1990**, *77*, 123.

(14) Burke, K.; Perdew, J. P.; Wang, Y. In *Electronic Density Functional Theory: Recent Progress and New Directions*; Dobson, J. F., Vignale, G., Das, M. P., Eds.; Plenum: New York, 1998.

(15) (a) Xiao, Z. L.; Hauge, R. H.; Margrave, J. L. *J. Phys. Chem.* **1991**, *95*, 2696. (b) Chertihin, G.V.; Andrews, L. *J. Am. Chem. Soc.* **1994**, *116*, 8322. (Ti + H_2)

(16) Lee, Y. K.; Manceron, L.; Papal, I. *J. Phys. Chem. A* **1997**, *101*, 9650.

(17) Eisch, J. J.; Gitua, J. N. *Organometallics* **2003**, *22*, 24.

(18) Chertihin, G.V.; Andrews, L. *J. Phys. Chem.* **1995**, *99*, 15004. (Zr, Hf + H_2)

(19) McGrady, G. S.; Downs, A. J.; McKean, D. C.; Haaland, A.; Scherer, W.; Verne, H.-P.; Volden, H. V. *Inorg. Chem.* **1996**, *35*, 4713. ((CH_3)$_2$$TiCl_2$)

(20) (a) Pyykko, P.; Desclaux, J. P. *Chem. Phys. Lett.* **1977**, *50*, 503. (b) Pyykko, P.; Snijders, J. G.; Baerends, E. *J. Chem. Phys. Lett.* **1981**, *83*, 432. (c) Ziegler, T.; Snijders, J. G.; Baerends, E. J. *J. Chem. Phys.* **1981**, *74*, 1271. (d) Pyykko, P. *Chem. Rev.* **1988**, *88*, 563. (relativistic effects)

JP801336D